Spin-dynamics study of the dynamic critical behavior of the three-dimensional classical Heisenberg ferromagnet

Kun Chen and D. P. Landau
Center for Simulational Physics, The University of Georgia, Athens, Georgia 30602
(Received 12 April 1993)

Using spin-dynamics techniques we have performed large-scale computer simulations of the dynamic behavior of the $L \times L \times L$ body-centered-cubic classical Heisenberg ferromagnet with $L \leq 40$ in the vicinity of the critical point T_c. The temporal evolutions of spin configurations were determined numerically from coupled equations of motion for individual spins by a fourth-order predictor-corrector method with initial spin configurations generated by Monte Carlo methods. The space- and time-displaced spin-spin correlation functions and their space-time Fourier transforms were calculated to determine the neutron-scattering functions. We developed a dynamic finite-size scaling theory for the neutron-scattering function at T_c and used it to extract the dynamic critical exponent z. Within our resolution limit, the value of z was estimated to be 2.478(28), in excellent agreement with the dynamic scaling prediction, and dynamic scaling was found to be valid for momentum transfer q up to 0.4π in the (1,0,0) direction.

I. INTRODUCTION

The static critical behavior of the three-dimensional classical Heisenberg ferromagnet has been well understood due to extensive studies carried out using a variety of approaches.[1-8] In a recent high-resolution Monte Carlo study,[8] the critical temperature and various static critical exponents for the simple cubic and body-centered-cubic systems were estimated with precision equivalent to, or better than, that found with any other method, and the hypothesis of universality for static properties[9] was substantiated once again. In contrast, the dynamic critical behavior is much less well understood. In analogy to static critical properties, dynamic critical behavior is expected,[10,11] by generalizing the static scaling laws[12,13] to dynamic critical phenomena, to be describable in terms of a dynamic critical exponent z, which depends on the conservation laws and which, in some cases, is related to static critical exponents.[14] In their classic work[15] on the theory of dynamic critical phenomena, Hohenberg and Halperin proposed a number of different dynamic universality classes based upon the conservation laws. By far the greatest amount of work has been carried out for class A models which have no conserved quantities. The best example in this class is the stochastic Ising model, for which the time dependent behavior has no true dynamics but is only relaxational. Extensive Monte Carlo simulations[16] have already been performed on this model but the results shed no light on the dynamic critical behavior found in most physical systems, although the model is itself of interest. A similar example in this class is the classical Heisenberg model treated stochastically via Monte Carlo simulations.[17] The classical Heisenberg ferromagnet of class J,[15] on the other hand, has true dynamics with a conserved order parameter. Spin variables in this model are of continuous degrees of freedom and their real-time dynamic behaviors are governed by coupled equations of motion. Using dynamic scaling Halperin and Hohenberg established a relation between the dynamic critical exponent and static critical exponents of this model,[11,15,18] which is supported mode-coupling theory[19-21] and renormalization-group theory.[22-26]

The europium compounds EuO and EuS are believed to be the two best model substances for the classical Heisenberg ferromagnet.[27,28] Exchange interactions between spins in these two ferromagnets are appreciable up to next-nearest neighbors; the nearest-neighbor interaction is ferromagnetic in both materials and the next-nearest-neighbor interaction is ferromagnetic in EuO but antiferromagnetic in EuS. Extensive experiments,[29-35] most of them using inelastic neutron-scattering techniques,[36] have been performed on the two materials to investigate critical dynamics and results were generally consistent with the dynamic scaling prediction.[37-40] More detailed comparisons between experimental results and those from high-temperature computer simulations[41] and from mode-coupling calculations,[42-44] both considering nearest-neighbor and next-nearest-neighbor interactions, have also been made and a satisfactory agreement was found. A stringent test of the dynamic scaling prediction by experiments, however, is hindered by the long-range dipolar interactions in the two materials. The long-range dipolar interactions cause a crossover from Heisenberg ferromagnet behavior to dipolar ferromagnet behavior and therefore a substantial change in results for the dynamic critical exponent.[45-48]

In this paper we present results of large-scale computer simulations of the dynamic critical behavior in the body-centered-cubic classical Heisenberg ferromagnet of up to 128 000 spins. Previous simulations treated system sizes and temporal evolution periods which were both more than an order of magnitude smaller than ours.[41,49,50] Since next-nearest-neighbor interactions and dipolar interactions are excluded in our model, we are able to test dynamic scaling more stringently. In Sec. II we define

our model and briefly review the dynamic scaling theory. We then describe our method and develop a dynamic finite-size scaling theory for the neutron-scattering function at the critical temperature. Results will be reported in Sec. III and conclusions drawn in Sec. IV.

II. MODEL AND METHODS

A. Model

The classical Heisenberg ferromagnet is defined by the Hamiltonian

$$\mathcal{H}=-J\sum_{\langle \mathbf{r}\mathbf{r}'\rangle}\mathbf{S}_{\mathbf{r}}\cdot S_{\mathbf{r}'}\ , \tag{1}$$

where $\mathbf{S}_{\mathbf{r}}=(S_{\mathbf{r}}^{x},S_{\mathbf{r}}^{y},S_{\mathbf{r}}^{z})$ is a three-dimensional classical spin of unit length at site $\mathbf{r}$ and J is the ferromagnetic coupling constant between nearest-neighbor spins $\mathbf{S}_{\mathbf{r}}$ and $\mathbf{S}_{\mathbf{r}'}$. We consider $L\times L\times L$ body-centered-cubic systems with periodic boundary conditions; the sum in Eq. (1) runs over all nearest-neighbor pairs of lattice sites. The dynamics of the spins is described by coupled equations of motion[49] and the time dependence of each spin $\mathbf{S}_{\mathbf{r}}(t)$ can be determined from integration of these equations.

B. Dynamic scaling

The space-displaced, time-displaced spin-correlation function and its space-time Fourier transform are fundamental in the study of critical spin dynamics.[36,51] The former is defined, with $k=x,y,$, or z, as

$$C^{k}(\mathbf{r}-\mathbf{r}',t)=\langle S_{\mathbf{r}}^{k}(t)S_{\mathbf{r}'}^{k}(0)\rangle-\langle S_{\mathbf{r}}^{k}(t)\rangle\langle S_{\mathbf{r}'}^{k}(0)\rangle\ , \tag{2}$$

where the angle brackets $\langle\cdots\rangle$ denote the ensemble average and the latter is given by

$$S^{k}(\mathbf{q},\omega)=\sum_{\mathbf{r},\mathbf{r}'}\exp[i\mathbf{q}\cdot(\mathbf{r}-\mathbf{r}')]\times\int_{-\infty}^{+\infty}\exp(i\omega t)C^{k}(\mathbf{r}-\mathbf{r}',t)\frac{dt}{\sqrt{2\pi}}\ . \tag{3}$$

The neutron-scattering function $S^{k}(\mathbf{q},\omega)$ is an experimental observable, for momentum transfer $\mathbf{q}$ and frequency transfer ω. Generally it depends on the correlation length ξ and may be written as[11]

$$S_{\xi}^{k}(\mathbf{q},\omega)=\frac{2\pi}{\omega_{m}(\mathbf{q},\xi)}S_{\xi}^{k}(\mathbf{q})f\left[\frac{\omega}{\omega_{m}(\mathbf{q},\xi)},\mathbf{q},\xi\right]\ , \tag{4}$$

where $\omega_{m}(\mathbf{q},\xi)$ is a characteristic frequency, $S_{\xi}^{k}(\mathbf{q})$ is given by the sum rule

$$S_{\xi}^{k}(\mathbf{q})=\int_{-\infty}^{+\infty}S_{\xi}^{k}(\mathbf{q},\omega)\frac{d\omega}{2\pi}\ , \tag{5}$$

and f is a shape function satisfying the normalization

$$\int_{-\infty}^{+\infty}f(x,\mathbf{q},\xi)dx=1\ . \tag{6}$$

The characteristic frequency $\omega_{m}(\mathbf{q},\xi)$ is a median frequency determined by the constraint

$$\int_{-\omega_{m}(\mathbf{q},\xi)}^{\omega_{m}(\mathbf{q},\xi)}S_{\xi}^{k}(\mathbf{q},\omega)\frac{d\omega}{2\pi}=\tfrac{1}{2}S_{\xi}^{k}(\mathbf{q})\ . \tag{7}$$

In the dynamic scaling theory it is assumed that the median frequency $\omega_{m}(\mathbf{q},\xi)$ is a homogeneous function of q and ξ, i.e.,

$$\omega_{m}(\mathbf{q},\xi)=q^{z}\Omega(q\xi)\ , \tag{8}$$

where z is the dynamic critical exponent, and that the function f depends only on the product of $q\xi$ but not on $\mathbf{q}$ and ξ separately. Therefore $S_{\xi}^{k}(\mathbf{q},\omega)$ is simplified as

$$S_{\xi}^{k}(\mathbf{q},\omega)=\frac{2\pi}{\omega_{m}(q,\xi)}S_{\xi}^{k}(\mathbf{q})f\left[\frac{\omega}{\omega_{m}(q,\xi)},q\xi\right]\ . \tag{9}$$

In the three-dimensional classical Heisenberg ferromagnet there exist propagating spin-wave excitations at a temperature T below the critical point T_{c}. The spin-wave frequency $\omega_{s}(\mathbf{q})$ is approximately proportional to q^{2} at small wave vectors[11,18,51]

$$\omega_{s}(\mathbf{q})=Dq^{2}\ , \tag{10}$$

where D is the spin-wave stiffness constant. It is predicted independently by the mode-coupling theory and hydrodynamic theory that

$$D\sim(1-T/T_{c})^{\nu-\beta}\ , \tag{11}$$

where ν and β are static critical exponents. Because the correlation length ξ diverges at T_{c}, $\xi\sim(1-T/T_{c})^{-\nu}$, dynamic scaling assumes that $\omega_{s}(\mathbf{q})$ and $\omega_{m}(\mathbf{q},\xi)$ behave in the same fashion and thus

$$D\sim(1-T/T_{c})^{(z-2)\nu}\ . \tag{12}$$

A comparison between Eq. (11) and Eq. (12) leads to the dynamic scaling law

$$z=2+(\nu-\beta)/\nu=3-\beta/\nu\ . \tag{13}$$

This dynamic scaling law was predicted independently by both the mode-coupling theory[19–21] and the renormalization-group theory.[22–26] In the paramagnetic region where $T>T_{c}$, there exist no propagating spin-wave excitations at long wavelengths but the relevant characteristic frequency $\omega_{m}(\mathbf{q})$ is still approximately proportional to q^{2},[11,18]

$$\omega_{m}(\mathbf{q})=D'q^{2}\ , \tag{14}$$

where D' is the spin-diffusion constant whose critical behavior is given by

$$D'\sim(T/T_{c}-1)^{\nu-\beta}\ . \tag{15}$$

If the temperature is high enough so that $q\xi\ll 1$, the shape function f is a simple Lorentzian centered at $\omega=0$ with a width given by characteristic frequency ω_{m}.

C. Simulations

Using Monte Carlo methods and spin-dynamics techniques, we simulated the dynamic behavior of the body-centered-cubic classical Heisenberg ferromagnet with $16\le L\le 40$ over a temperature range around the critical point,[8] $T_{c}=2.054\,241J$. Individual simulations consisted of two major stages as described below.

First, Monte Carlo methods were employed to sample an equilibrium spin configuration from a canonical ensemble. We used a fully vectorized checkerboard algorithm which hybridized the Metropolis method[52] and the overrelaxation method.[53,54] Every hybrid step consisted of two Metropolis steps and eight overrelaxation steps sequentially. (Such an algorithm reduces critical slowing down quite significantly.[55]) At the critical point, for all system sizes we investigated, the measured integrated autocorrelation time for the total energy and that for the magnetization are both smaller than 100 hybrid steps. We discarded the first 1000 hybrid steps for equilibration.

Then we solved the coupled equations of motion numerically. We used initial spin configurations generated by the Monte Carlo algorithm and a vectorized fourth-order predictor-corrector method[56] to perform the integration. We chose a Cartesian coordinate system in the spin space such that its z axis was parallel to the magnetization of the spin configuration and carried the integration out to a maximum time $t_{\max}=120J^{-1}$ with a time step $\Delta=0.01J^{-1}$. The total energy, the magnetization, and the length of individual spins should be constant in time, and indeed at T_c with $L=40$, a maximum variation in the fifth digit of the total energy and in the sixth digit of the length of individual spins was observed. For the magnetization the variation in the z component, whose value was typically about 0.15, occurred in the fourteenth digit, while the magnitudes of both x and y components remained smaller than 1×10^{-14} throughout the integration. We also performed additional integrations for some initial spin configurations to the same $t_{\max}$ with $\Delta=0.005J^{-1}$ and found that the difference in data obtained was smaller than the statistical fluctuations resulting from different initial spin configurations.

Because $S(q,\omega)$ provides access to the dynamic behavior, it would be ideal if all values of $C^k(\mathbf{r}-\mathbf{r}',t)$ could be stored so that the neutron-scattering function could be calculated later for any $\mathbf{q}$ and ω of interest. However, in a single simulation for a system size L, the number of calculations involved in computing all possible spin correlations of a time-displacement range of $100J^{-1}$ at time intervals of $0.1J^{-1}$ is roughly about $1\times10^4L^6$ and the number of data thus generated is about $3\times10^3L^3$. Therefore it is impractical to compute and store all spin correlation functions for systems as large as $L=40$ because of currently limited computer resources. We developed a vectorized algorithm to calculate partial spin sums "on the fly" to substantially reduce the storage needs as well as CPU time. The price we paid was to limit ourself to a single $\mathbf{q}$ direction. The basic idea of the algorithm is rather straightforward. If the direction is chosen to be, say, $\mathbf{q}=(q,0,0)$ with q determined by the periodic boundary conditions,

$$q=\frac{2\pi n}{L}\ ,\quad n=\pm1,\pm2,\ldots,\pm(L-1),L\ , \tag{16}$$

excluding $q=0$, the spatial Fourier transform in Eq. (3) can be simplified as

$$\sum_{\mathbf{r},\mathbf{r}'}\exp[iq(r_x-r_x')]S_{\mathbf{r}}^k(t)S_{\mathbf{r}'}^k(0) = \sum_{r_x,r_x'}\exp[iq(r_x-r_x')]\times\left[\sum_{r_y,r_z}S_{\mathbf{r}}^k(t)\right]\left[\sum_{r_y',r_z'}S_{\mathbf{r}'}^k(0)\right]\ , \tag{17}$$

where the subscripts in r or r' denote the Cartesian components. Therefore we can compute $[\sum_{r_y,r_z}S_{\mathbf{r}}^k]$ as a function of r_x for each measurement during the simulation and calculate $\{[\sum_{r_y,r_z}S_{\mathbf{r}}^k(t)][\sum_{r_y',r_z'}S_{\mathbf{r}'}^k(0)]\}$ as a function of t for each r_x at the end. Because of translational invariance of the spin-spin correlation function in time, we averaged the result over 201 different time-starting points evenly spaced by $0.1J^{-1}$,

$$\sum_{r_y,r_z}S_{\mathbf{r}}^k(t)\sum_{r_y',r_z'}S_{\mathbf{r}'}^k(0) = \frac{1}{201}\sum_{j=0}^{200}\left[\sum_{r_y,r_z}S_{\mathbf{r}}^k(t+0.1j)\right]\left[\sum_{r_y',r_z'}S_{\mathbf{r}'}^k(0.1j)\right]\ , \tag{18}$$

for $0\le t\le t_{\text{cutoff}}$ with $t_{\text{cutoff}}=100J^{-1}$. Since all three Cartesian spatial directions are equivalent by symmetry, we only store the results from Eq. (18), as a function of the space displacement along an axis direction and the time displacement, averaged over the three Cartesian spatial directions.

Multiple simulations were performed for all systems in order to take the ensemble average introduced in Eq. (2). We used 100 equilibrium spin configurations for all system sizes at T_c and 20 to 40 at each temperatures other than T_c for the averages. We also averaged results for $k=x$ and y, since the magnetization is a conserved vector along the z direction in the spin space so that the neutron-scattering function $S_\xi^k(\mathbf{q},\omega)$ can be regrouped in terms of symmetry as a longitudinal component

$$S_\xi^{\parallel}(\mathbf{q},\omega)=S_\xi^z(\mathbf{q},\omega) \tag{19}$$

and a transverse component

$$S_\xi^{\perp}(\mathbf{q},\omega)=\tfrac{1}{2}[S_\xi^x(\mathbf{q},\omega)+S_\xi^y(\mathbf{q},\omega)]\ . \tag{20}$$

Note that, when the magnetization vanishes in the high-temperature region, such a regrouping is unnecessary because the system is now rotationally invariant so that the x, y, and z directions are equivalent by symmetry. Instead, we only need to consider

$$S_\xi(\mathbf{q},\omega)=\tfrac{1}{3}[S_\xi^x(\mathbf{q},\omega)+S_\xi^y(\mathbf{q},\omega)+S_\xi^z(\mathbf{q},\omega)]\ . \tag{21}$$

D. Dynamic finite-size scaling

Due to limited computer resources, there are two major practical limitations on the computer simulation of dynamic behavior, i.e., finite evolution time and finite sys-

tem size. The finite time cutoff can introduce many oscillations into the result of the Fourier transform, Eq. (3). These oscillations, however, can be smoothed out by convoluting the spin-spin correlation function with a resolution function in frequency,[41,57,58] which is one dimensional and equivalent to the energy resolution in neutron-scattering experiments. If we use a Gaussian resolution function, the smoothed neutron-scattering function is

$$\bar{S}^k_\xi(\mathbf{q},\omega)\equiv\sum_{\mathbf{r},\mathbf{r}'}\exp[i\mathbf{q}\cdot(\mathbf{r}-\mathbf{r}')]\int_{-t_{\rm cutoff}}^{+t_{\rm cutoff}}\exp(i\omega t)C^k(\mathbf{r}-\mathbf{r}',t)\exp\left[-\frac{(t\delta_\omega)^2}{2}\right]\frac{dt}{2\pi}$$
$$\approx\frac{1}{\sqrt{2\pi}\delta_\omega}\int_{-\infty}^{+\infty}S^k_\xi(\mathbf{q},\omega')\exp\left[-\frac{(\omega-\omega')^2}{2\delta_\omega^2}\right]d\omega' , \tag{22}$$

where δ_ω is a parameter determining the resolution in frequency and needs to be chosen properly such that effects of the cutoff in the evolution time can be neglected. Note that

$$\bar{S}^k_\xi(\mathbf{q})\equiv\int_{-\infty}^{+\infty}\bar{S}^k_\xi(\mathbf{q},\omega)\frac{d\omega}{2\pi}\approx\int_{-\infty}^{+\infty}S^k_\xi(\mathbf{q},\omega)\frac{d\omega}{2\pi}\equiv S^k_\xi(\mathbf{q}) . \tag{23}$$

The finite-size effect, on the other hand, can be used to extract the dynamic critical exponent as has been done in the static situation.[8,59] In a finite system the divergence of the correlation length ξ in the critical region is limited by the linear dimension of the system, L, Replacing ξ by L in the previous equations, we get, for the finite system,

$$\bar{S}^k_L(\mathbf{q},\omega)\approx\omega^{-1}\bar{S}^k_L(\mathbf{q})F\left[\frac{\omega}{\omega_m(q,L)},qL,\frac{\delta_\omega}{\omega_m(q,L)}\right] , \tag{24}$$

where F is an unknown function which depends on the shape function f. Using Eq. (8) we can further express $\bar{S}^k_L(\mathbf{q},\omega)$ in a scaling form,

$$\frac{\omega\bar{S}^k_L(\mathbf{q},\omega)}{\bar{S}^k_L(\mathbf{q})}=G(\omega L^z,qL,\delta_\omega L^z) , \tag{25}$$

where G in another unknown function. We can also define a median frequency $\bar{\omega}_m$ for the smoothed neutron-scattering function $\bar{S}^k_L(\mathbf{q},\omega)$,

$$\int_{-\omega_m}^{+\bar{\omega}_m}\bar{S}^k_L(\mathbf{q},\omega)\frac{d\omega}{2\pi}=\tfrac{1}{2}\bar{S}^k_L(\mathbf{q}) . \tag{26}$$

It can be shown that

$$\bar{\omega}_m=L^{-z}\bar{\Omega}(qL,\delta_\omega L^z) , \tag{27}$$

where the explicit form for function $\bar{\Omega}$ is also unknown. Since $\bar{S}^k_L(\mathbf{q},\omega)$, $\bar{S}^k_L(\mathbf{q})$ and $\bar{\omega}_m$ can be estimated in simulations, Eqs. (25) and (27) provide an approach to test dynamic scaling and to estimate the dynamic critical exponent z.

In the experiments on critical spin dynamics, the characteristic frequency $\bar{\omega}_m$ was extracted from a limited number of experimental data points with the shape function given in an explicit analytical form.[29–35] Several different shape functions have been proposed and the interpretation of the experimental results might be affected by the choice.[39] This difficulty, however, is avoided in simulations, since the characteristic frequency can be estimated directly from Eq. (26). We used Simpson's rule[56] for the numerical integrations involved in Eqs. (22), (23), and (26). For the time integration in Eq. (22) we used a time interval of $0.1J^{-1}$ but no difference was found using an interval of $0.2J^{-1}$.

We used Eq. (27), rather than Eq. (25), to determine the dynamic critical exponent z. A major reason was that individual points in $\bar{S}^k_L(\mathbf{q},\omega)$ suffered from statistical fluctuations due to limited number of samples, but these fluctuations can be more or less averaged out in determining $\bar{\omega}_m$ by the integration and the normalization in Eq. (26). Because the function $\bar{\Omega}$ in Eq. (27) was unknown, we extracted z by self-consistent iterations. A key point of our scheme was to keep the two arguments of $\bar{\Omega}$, and therefore the value of $\bar{\Omega}$ itself, constant in each iteration for all system sizes, so that

$$\bar{\omega}_m\sim L^{-z} . \tag{28}$$

For the first argument of $\bar{\Omega}$, we fixed the product of q and L, or more precisely, the value of n as defined in Eq. (16), since we were interested in only those q values determined by the periodic boundary conditions. For the second argument, we chose

$$\delta_\omega=0.025\left[\frac{40}{L}\right]^z , \tag{29}$$

where the resolution coefficient 0.025, in units of J, was obtained empirically. This value provides a good compromise between effectively reducing the oscillations due to $t_{\rm cutoff}=100J^{-1}$ and not excessively broadening the structure of the neutron-scattering function. In a single iteration we first picked an initial value $z^{(0)}$ for z and used this to determine δ_ω by Eq. (29) for different L. We then calculated $\bar{S}^k_L(\mathbf{q},\omega)$ and $\bar{\omega}_m$ from Eqs. (22) and (26) for different combinations of L and q constrained by the fixed n value. A new estimate, $z^{(1)}$, was finally extracted from the simple relation Eq. (28), which is a special case of Eq. (27) with the function $\bar{\Omega}$ being kept constant. We also tried another value, $0.035J$, for the resolution coefficient in Eq. (29) and found that it did not lead to a statistically different estimate for z although it did significantly broaden and smooth the structure of the neutron-scattering function.

III. RESULTS

We present first a qualitative comparison of the dynamic behavior at two different temperatures, one close to and the other far below the critical point. Typical results for the transverse component $S_L^{\perp}(\mathbf{q},\omega)$ and the longitudinal component $S_L^{\parallel}(\mathbf{q},\omega)$ of the neutron-scattering function are given in Fig. 1 for two q values. The resolution shown in the plots is obtained with $\delta_\omega=0.025J$. Small wiggles remaining in the figure are noise due to finite number of samples. At the lower temperature, $S_L^{\perp}(\mathbf{q},\omega)$ exhibits a resolution-limited spin-wave peak for every q value given by Eq. (16). As q increases the peak shifts toward high frequencies and its height decreases rapidly but its width remains constant. The dispersion relation determined from the peak position is plotted in Fig. 2 and agrees very well with the prediction from the linear spin-wave approximation.[51] The small deviations visible near the Brillouin-zone boundary are presumably due to the finite temperature of the system, not finite-size effects, because the dispersion relation for $L=20$ at the same temperature shows similar results. At the higher temperature, $S_L^{\perp}(\mathbf{q},\omega)$ also reveals similar spin-wave excitations; however, the peak is higher and broader, and is asymmetric with some intensity even at $\omega=0$. As q increases its height decreases and its width increases, until, because of increasing statistical fluctuations, only a part of the dispersion relation can be estimated. It is clear that the spin-wave stiffness constant decreases as the temperature rises, as one would expect from Eq. (11). $S_L^{\parallel}(\mathbf{q},\omega)$, on the other hand, behaves in a totally different way. At the lower temperature, it shows almost nothing within our resolution limit. At the higher temperature, a broad peak appears around $\omega=0$ for small q. As q increases the broad peak seemingly breaks into two parts, a resolution-limited central peak and a q-dependent broad peak, as demonstrated in Fig. 1. Presumably the central peak is due to the elastic diffusive scattering associated with the long-range spatial correlation between spins, which develops as the critical point is approached, and the other one is due to the residual spin-wave excitations. Remember that the magnetization is in the z direction, i.e., the longitudinal direction. At the critical point, the magnetization survives in a finite system because of finite-size effects, and, consequently, the transverse component and its longitudinal counterpart still behave differently. In Fig. 3, $S(q,\omega)$ is shown for four different system sizes with the same q and δ_ω. Because of statisti-

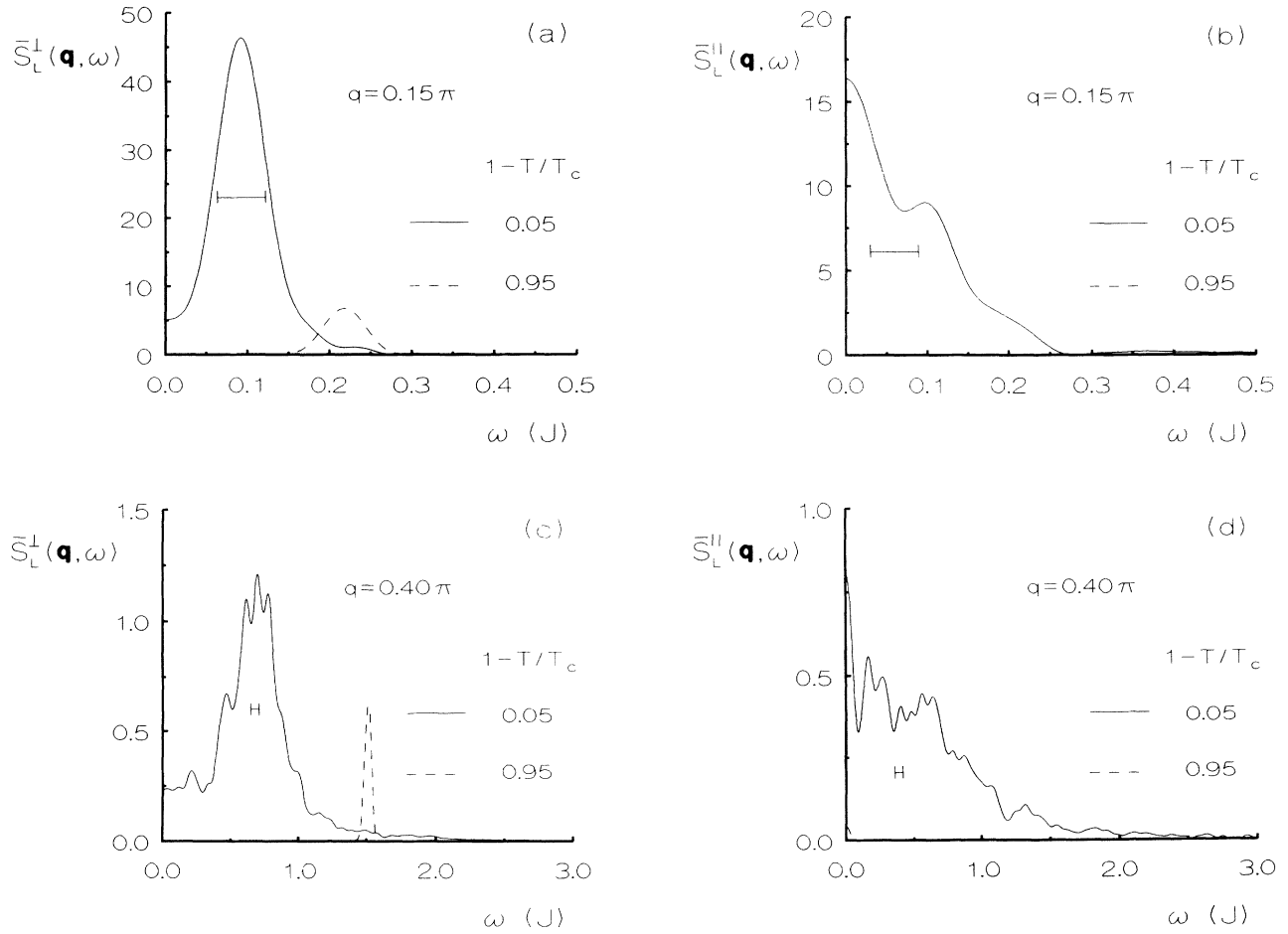

FIG. 1. Transverse and longitudinal neutron-scattering functions at two different temperatures for $L=40$. The horizontal bar represents the "instrumental peak width" due to the Gaussian resolution function with $\delta_\omega=0.025J$. At the lower temperature, $(1-T/T_c)=0.95$, $S_L^{\parallel}(q,\omega)$ shows no structure on this scale.

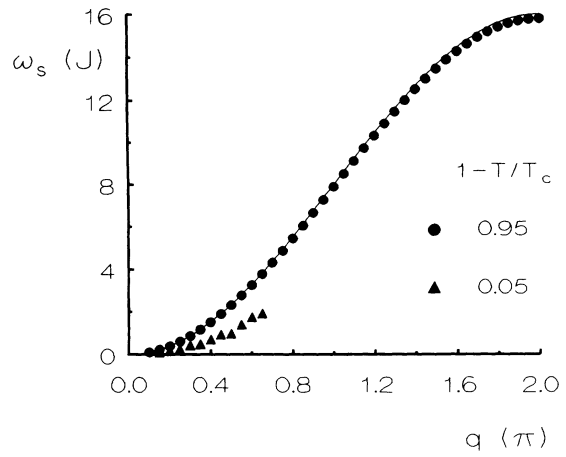

FIG. 2. Dispersion relations for spin-wave excitations in the x-y plane for $L=40$ and $\delta_\omega=0.025J$ at two different temperatures. Because of statistical fluctuations, only a portion of the dispersion relation at $(1-T/T_c)=0.05$ can be estimated from the peak position. The solid curve, given by $16\sin^2(q/4)$, is the prediction from the linear spin-wave approximation. The estimated error bars are within the symbols.

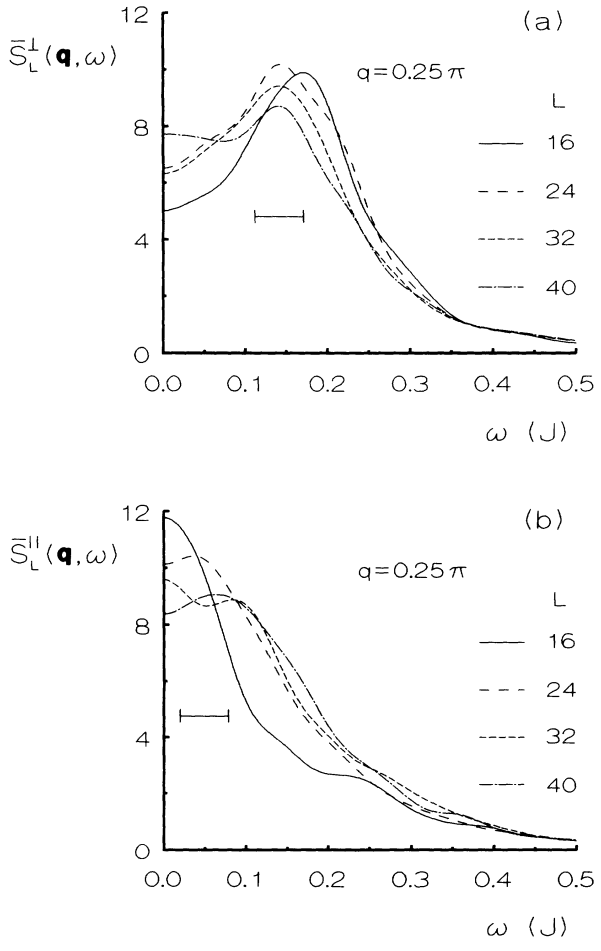

FIG. 3. Transverse and longitudinal neutron-scattering functions at the critical point. The horizontal bar represents the "instrumental peak width" due to the Gaussian resolution function with $\delta_\omega=0.025J$.

cal fluctuations, finite-size effects are not so obvious; there are, however, systematic shifts in the peak position and in the magnitude of both wings of the transverse component. For the longitudinal part we can also observe a systematic change in the intensity at $\omega=0$. As we will see later, a better way to look into the finite-size behavior is to draw a scaling plot according to Eq. (25) by fixing the values of qL and $\delta_\omega L^z$. Finally, in Fig. 4 we display $S(q,\omega)$ [see Eq. (21)] for $L=40$ at $T=2.0T_c$. In the figure the estimated error bars are shown unless they are smaller than the size of the points. The dashed line shown in the figure is obtained by adjusting the total intensity and the width of the Lorentzian function to best fit the data. At this high temperature, $S(q,\omega)$ can be well described by a simple Lorentzian function convoluted with a Gaussian resolution function.

Because the behavior of $S^{\perp}_L(\mathbf{q},\omega)$ in the critical region is not complicated by the residual magnetization as is the longitudinal one, we will concentrate only on the transverse component in our following studies of the critical spin dynamics. In Fig. 5 we show the temperature dependence of the spin-wave frequency, read directly from the peak position at two q values for $L=20$ and 40, in the vicinity of the critical point. In this figure the estimated error bars are plotted unless they are smaller than the size of the points. As one can see from the figure, there is a systematic rounding for both systems when $(1-T/T_c)$ is smaller than 0.03. This is clearly due to finite-size effects, because this temperature range is so close to the critical point that the correlation length becomes limited by the linear dimension of the system. On the other hand, finite-size effects seem to be negligible for the system with $L=40$ in the temperature region $(1-T/T_c)\geq 0.03$. According to Eqs. (10) and (11), if finite-size effects are negligible and the q value is small and fixed, the spin-wave frequency should vary as $(1-T/T_c)^{\nu-\beta}$. Curve fits to data with $L=40$ and $(1-T/T_c)\geq 0.03$ yield two consistent

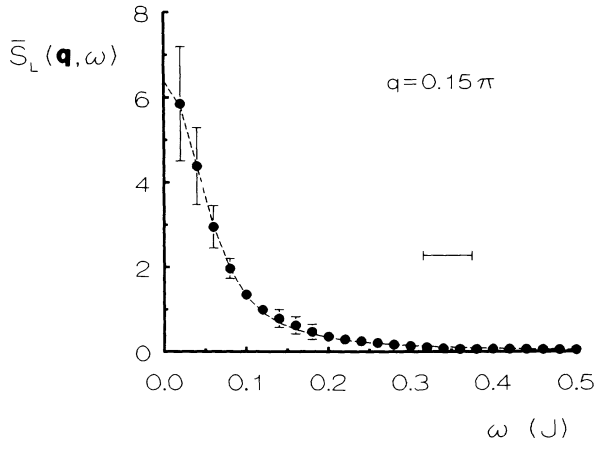

FIG. 4. The neutron-scattering function for $L=40$ at $T=2.0T_c$. Simulational results (solid dots) are well described by a Lorentzian function convoluted with a Gaussian resolution function (dashed line). The horizontal bar represents the "instrumental peak width" due to the Gaussian resolution function with $\delta_\omega=0.025J$.

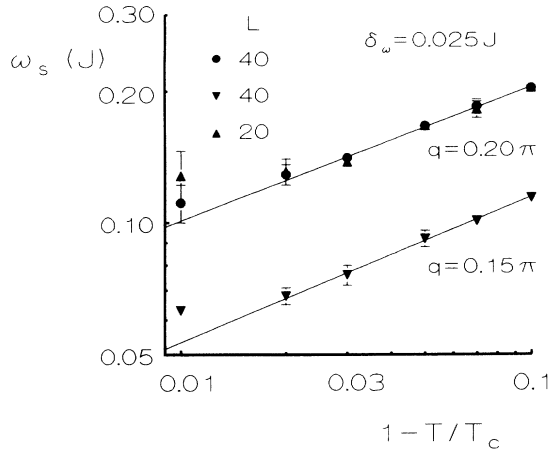

FIG. 5. Log-log plot of temperature dependence of spin-wave frequency. The data points for $L=20$ are used only to check finite-size effects.

estimates for the exponent $(\nu-\beta)$, 0.301(24) from the top straight line, and 0.331(33) from the bottom one. From their mean we obtain $(\nu-\beta)=0.316(21)$. In the recent high-resolution Monte Carlo study of the static critical behavior,[8] the static critical exponents ν and β are estimated to be 0.7048(30) and 0.3639(35), respectively, which gives $(\nu-\beta)=0.3409(65)$. Within their respective error bars, the estimates from static and dynamic properties agree.

The dynamic critical exponent z can be extracted from $\bar{\omega}_m$ by the iteration scheme described in the previous section. The self-consistency of the iteration result for $n=2$ and that for $n=3$ is demonstrated in Fig. 6 where the size dependence of $\bar{\omega}_m$ is plotted on a logarithmic scale. When not shown, the estimated error bars for individual points are smaller than the size of the points. In the inset

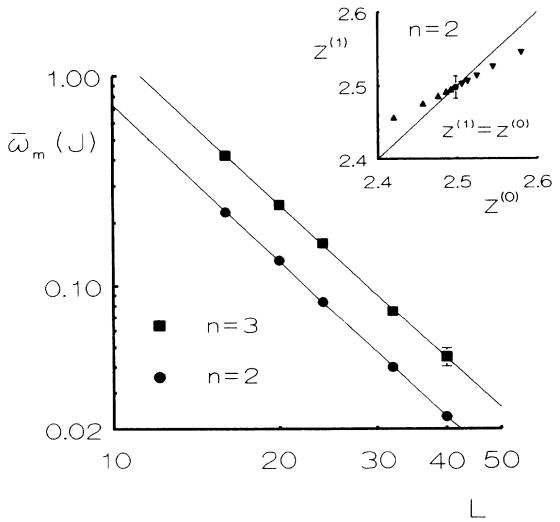

FIG. 6. Finite-size scaling plot for $\bar{\omega}_m$ (with $qL=$const, $\delta_\omega L^z=$const) using the converged value for z. Two independent iteration sequences for $n=2$ are shown in the inset by different types of solid triangles and the converged value by the solid dot.

to this figure results of individual iterations with $n=2$ are shown. The largest and smallest values of $z^{(0)}$ in the inset are two different initial values for two independent iterations which converge to the same value of $z=2.498$. Also shown in the inset is a typical error bar obtained in the fitting to Eq. (28). From the figure we have the value of z to be 2.498(15) for $n=2$ and 2.458(27) for $n=3$. Within their respective error bars, the two estimates for z agree; combining them, we obtain $z=2.478(28)$. Experimentally, z was estimated to be 2.50 ± 0.07,[33] which is consistent with our estimate but with a larger uncertainty.

In accordance with Eq. (25), the dynamic finite-size scaling behavior of the transverse neutron-scattering function is plotted in Fig. 7 for $n=2$, where δ_ω is given by Eq. (29) with $z=2.478$. The estimated error bars for individual data points are shown unless they are smaller than the size of the symbols. Within their respective error bars, data points collapse onto the same curve. Similar scaling behavior exists for the case of $n=3$. These results, therefore, support our estimate for z.

Based on these results, we can now examine the dynamic scaling law, Eq. (13). With $\nu=0.7048(30)$ and $\beta=0.3639(35)$,[8] which were obtained from the high-resolution Monte Carlo study of the static critical behavior, the dynamic scaling law predicts $z=2.4837(72)$. Using the dynamic result $(\nu-\beta)=0.316(21)$ from Fig. 5, together with the static result for ν, we predict $z=2.448(32)$. Within their respective error bars, these two predictions are consistent and in excellent agreement with the dynamic scaling value $z=2.478(28)$. We, therefore, believe the dynamic scaling law is valid.

It is important to know the region where dynamic scaling is valid. In Fig. 8 we plot $\bar{\omega}_m$, obtained with δ_ω given by Eq. (29) and $z=2.478$, for several values of n. The estimated error bars are all smaller than the size of the points. The straight lines, all going through the origin, are linear fits to three data points for the systems with $L=24$, 32, and 40. If dynamic scaling is valid, according to Eq. (28), data points for $L=16$ and 20 should fall on

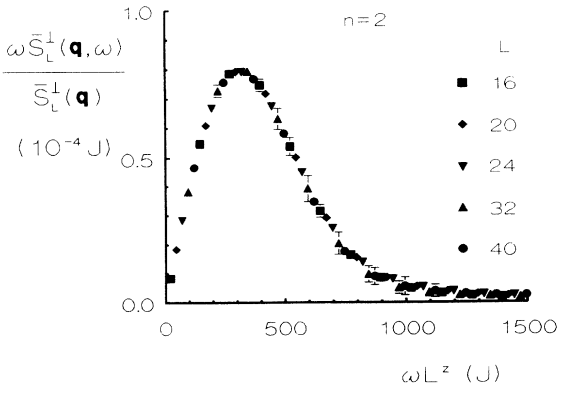

FIG. 7. Scaling behavior of the transverse neutron-scattering function for $n=2$ and $z=2.478$. The maximum value of q involved is 0.25π for $L=16$.

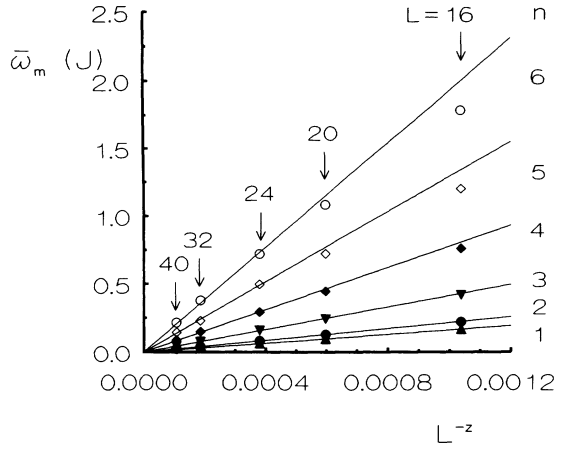

FIG. 8. Size dependence of the median frequency $\bar{\omega}_m$ at the critical point with δ_ω given by Eq. (29) and $z=2.478$.

one of these straight lines, within their respective error bars. From the figure we can see this is the case for $n=1$, 2, and 3. The maximum q value involved here is $q=0.4\pi$ for $n=4$ and $L=20$. For $n=4$, 5, and 6, it seems that points corresponding to $q \geq 0.5\pi$, e.g., $n=4$ for $L=16$ and $n=5$ for $L=20$, deviate from the lines, indicating the failure of dynamic scaling.

IV. CONCLUSIONS

The dynamic critical properties of the classical Heisenberg ferromagnet have been studied in our large-scale computer simulations. Using a combination of Monte Carlo methods and spin-dynamics techniques, we have solved coupled equations of motion, for systems with as many as 128 000 classical spins, to yield true dynamics. We developed a scheme of partial spin sums "on the fly," which makes it possible to keep intermediate data of the space- and time-displaced spin-spin correlation functions permanently for later analyses. We also developed a dynamic finite-size scaling theory for the neutron-scattering function and found dynamic scaling to be valid for $(q,0,0)$ with q up to 0.4π and the dynamic critical exponent $z=2.478(28)$. This estimate for z is in excellent agreement with the prediction from the dynamic scaling law using static critical exponents.

We were able to examine the dynamic scaling theory and extract the dynamic critical exponent without any consideration of the explicit expression for the shape function at the critical point, although the expression itself is crucial for successful interpretation of experiments. In order to use computer simulations to perform a stringent test of existing analytical expressions for the shape function, it is necessary to incorporate finite-size scaling explicitly into the analytical expressions for the shape function and to improve statistics substantially on the individual data points of the neutron-scattering function. These, in fact, are not trivial: The former calls for more theoretical effort and the latter demands better algorithms and much more CPU time.

ACKNOWLEDGMENTS

We are indebted to K. Binder for helpful discussions. Computer simulations were carried out on the CRAY Y-MP/832 and CRAY C90 at the Pittsburgh Supercomputing Center. This research was supported in part by NSF Grant No. DMR-9100692.

[1]D. S. Ritchie and M. E. Fisher, Phys. Rev. B **5**, 2668 (1972).
[2]S. McKenzie, C. Domb, and D. L. Hunter, J. Phys. A **15**, 3899 (1982).
[3]J. C. LeGuillou and J. Zinn-Justin, Phys. Rev. B **21**, 3976 (1980); J. Phys. (Paris) Lett. **46**, L137 (1985).
[4]M. Ferrer and A. Hamid-Aidinejad, Phys. Rev. B **34**, 6481 (1986).
[5]M. P. Nightingale and H. W. J. Blöte, Phys. Rev. Lett. **60**, 1562 (1988).
[6]P. Peczak, A. M. Ferrenberg, and D. P. Landau, Phys. Rev. B **43**, 6087 (1991).
[7]C. Holm and W. Janke, Phys. Lett. A **173**, 8 (1993).
[8]K. Chen, A. M. Ferrenberg, and D. P. Landau, J. Appl. Phys. **73**, 5488 (1993); Phys. Rev. B **48**, 3249 (1993).
[9]L. P. Kadanoff, in *Critical Phenomena,* Proceedings of the International School of Physics "Enrico Fermi" Course 51, edited by M. S. Green (Academic, New York, 1971), p. 100.
[10]R. A. Ferrell, N. Menyhárd, H. Schmidt, F. Schwabl, and P. Szépfalusy, Phys. Rev. Lett. **18**, 891 (1967); Ann. Phys. (N.Y.) **47**, 565 (1968).
[11]B. I. Halperin and P. C. Hohenberg, Phys. Rev. Lett. **19**, 700 (1967); Phys. Rev. **177**, 952 (1969).
[12]B. Widom, J. Chem. Phys. **43**, 3898 (1965).
[13]L. P. Kadanoff, Physics **2**, 263 (1966).
[14]B. I. Halperin, P. C. Hohenberg, and S. Ma, Phys. Rev. Lett. **29**, 1548 (1972); Phys. Rev. B **10**, 139 (1974).
[15]P. C. Hohenberg and B. I. Halperin, Rev. Mod. Phys. **49**, 435 (1977).
[16]S. Wansleben and D. P. Landau, Phys. Rev. B **43**, 6006 (1991), and references therein.
[17]P. Peczak and D. P. Landau, J. Appl. Phys. **67**, 5427 (1990).
[18]B. I. Halperin and P. C. Hohenberg, Phys. Rev. **188**, 898 (1969).
[19]H. Wagner, Phys. Lett. A **33**, 58 (1970).
[20]J. Hubbard, J. Phys. C **4**, 53 (1971).
[21]K. Kawasaki, J. Phys. Chem. Solids **28**, 1277 (1967); Ann. Phys. (N.Y.) **61**, 1 (1970); Prog. Theor. Phys. **39**, 1133; **40**, 11; **40**, 706 (1968); in *Phase Transitions and Critical Phenomena,* edited by C. Domb and M. S. Green (Academic, New York, 1976), Vol. 5a, p. 165.
[22]S. Ma and G. F. Mazenko, Phys. Rev. Lett. **33**, 1383 (1974); Phys. Rev. B **11**, 4077 (1975).
[23]K. Kawasaki, Prog. Theor. Phys. **54**, 1665 (1975).
[24]R. Bausch, H. K. Janssen, and H. Wagner, Z. Phys. B **24**, 113 (1976).
[25]V. Dohm, Solid State Commun. **20**, 657 (1976).
[26]H. K. Janssen, Z. Phys. B **23**, 377 (1976).
[27]L. Passell, O. W. Dietrich, and J. Als-Nielsen, Phys. Rev. B **14**, 4897 (1976).
[28]J. Als-Nielsen, O. W. Dietrich, and L. Passell, Phys. Rev. B **14**, 4908 (1976).
[29]O. W. Dietrich, J. Als-Nielsen, and L. Passell, Phys. Rev. B

14, 4923 (1976).
[30]H. G. Bohn, A. Kollmar, and W. Zinn, Phys. Rev. B **30**, 6504 (1984).
[31]P. Böni, G. Shirane, H. G. Bohn, and W. Zinn, J. Appl. Phys. **61**, 3397 (1987); **63**, 3089 (1988).
[32]J. W. Lynn, Phys. Rev. Lett. **52**, 775 (1984).
[33]P. Böni and G. Shirane, Phys. Rev. B **33**, 3012 (1986).
[34]P. Böni, M. E. Chen, and G. Shirane, Phys. Rev. B **35**, 8449 (1987).
[35]F. Mezei, J. Magn. Magn. Mater. **45**, 67 (1984); Physica **136B**, 417 (1986).
[36]J. Als-Nielsen, in *Phase Transitions and Critical Phenomena,* Ref. 21, p. 87.
[37]S. W. Lovesey and R. D. Williams, J. Phys. C **19**, L253 (1986).
[38]U. Balucani, P. Carra, S. W. Lovesey, M. G. Pini, and V. Tognetti, J. Phys. C **20**, 3953 (1987).
[39]R. Folk and H. Iro, Phys. Rev. B **32**, 1880 (1985); **34**, 6571 (1986).
[40]H. Iro, Z. Phys. B **68**, 485 (1987).
[41]R. Chaudhury and B. S. Shastry, Phys. Rev. B **37**, 5216 (1988).
[42]P. A. Lindgård, J. Appl. Phys. **53**, 1861 (1982); Phys. Rev. B **27**, 2980 (1983).
[43]A. P. Young and B. S. Shastry, J. Phys. C **15**, 4547 (1982).
[44]A. Cuccoli, V. Tognetti, and S. W. Lovesey, Phys. Rev. B **39**, 2619 (1989).
[45]M. E. Fisher and A. Aharony, Phys. Rev. Lett. **30**, 559 (1973); Phys. Rev. B **8**, 3342 (1973).
[46]R. Raghavan, and D. L. Huber, Phys. Rev. B **14**, 1185 (1976).
[47]J. Kötzler, Phys. Rev. Lett. **51**, 833 (1983).
[48]E. Frey and F. Schwabl, Phys. Lett. A **123**, 49 (1987); Z. Phys. B **71**, 35 (1988).
[49]R. E. Watson, M. Blume, and G. H. Vineyard, Phys. Rev. **181**, 811 (1969).
[50]M. Takahashi, J. Phys. Soc. Jpn. **52**, 3592 (1983).
[51]S. W. Lovesey, *Theory of Neutron Scattering from Condensed Matter* (Clarendon, Oxford, 1984).
[52]N. Metropolis, A. W. Rosenbluth, M. N. Rosenbluth, A. H. Teller, and E. Teller, J. Chem. Phys. **21**, 1087 (1953).
[53]F. R. Brown and T. J. Woch, Phys. Rev. Lett. **58**, 2394 (1987).
[54]M. Creutz, Phys. Rev. D **36**, 515 (1987).
[55]P. Peczak and D. P. Landau, Phys. Rev. B **47**, 14 260 (1993).
[56]See, e.g., R. L. Burden, J. D. Fairas, and A. C. Reynolds, *Numerical Analysis* (Prindle, Weber, and Schmidt, Boston, 1981).
[57]T. R. Koehler and P. A. Lee, J. Comput. Phys. **22**, 319 (1976).
[58]R. W. Gerling and D. P. Landau, Phys. Rev. B **41**, 7139 (1990).
[59]See, e.g., *Finite-Size Scaling and Numerical Simulation of Statistical Systems,* edited by V. Privman (World Scientific, Singapore, 1990).